Acta Biomaterialia 114 (2020) 460–470

Contents lists available at ScienceDirect

Acta Biomaterialia

journal homepage: www.elsevier.com/locate/actbio

Full length article

Chondroitin-4-sulfate transferase-1 depletion inhibits formation of a proteoglycan-rich layer and alters immunotolerance of bone marrow mesenchymal stem cells on titanium oxide surfaces

Hisanobu Kamio[a], Shuhei Tsuchiya[b,*], Kensuke Kuroda[c], Masazumi Okido[c], Kazuto Okabe[b], Yuya Ohta[a], Naoto Toyama[a], Hideharu Hibi[a]

[a] Department of Oral and Maxillofacial Surgery, Nagoya University Graduate School of Medicine, 65 Tsurumai-cho, Showa-ku, Nagoya, Aichi 466-8550, Japan
[b] Department of Oral and Maxillofacial Surgery, Nagoya University Hospital, 65 Tsurumai-cho, Showa-ku, Nagoya, Aichi 466-8550, Japan
[c] EcoTopia Science Institute, Nagoya University, Furo-cho, Chikusa-ku, Nagoya, Aichi 464-8603, Japan

ARTICLE INFO

Article history:
Received 13 March 2020
Revised 21 June 2020
Accepted 16 July 2020
Available online 21 July 2020

Keywords:
Osseointegration
Chondroitin-4-sulfate transferase-1
Titanium oxides
Dental implant

ABSTRACT

Successful osseointegration is essential for dental implants. However, the complete molecular mechanism of osseointegration remains to be elucidated. In this study, we focused on the proteoglycan (PG)-rich layer between titanium oxides (TiOx) and bone, and chondroitin-4-sulfate transferase-1 (C4ST-1), which forms the sugar chain in PGs. Human bone marrow mesenchymal stem cells (hBMSCs) depleted of C4ST-1 were cultured on titanium (Ti) plates, and the interface between hBMSCs and TiOx was analyzed using transmission electron microscopy. Immunotolerance, proliferation, initial adhesion, and calcification of the cells were analyzed *in vitro*. At 14 days of cultivation, a PG-rich layer was observed between hBMSCs and TiOx. However, the PG-rich layer was reduced in C4ST-1-depleted hBMSCs on TiOx. Real-time RT-PCR showed that conditioned media increased the levels of expression of M1-macrophage markers in human macrophages. However, depletion of C4ST-1 did not affect calcification, cell proliferation, or initial cell adhesion on Ti plates. These results suggested that C4ST-1 in hBMSCs affects their immunotolerance and alters the formation of PG-rich layer formation on TiOx.

Statement of significance

Treatment of dental implants requires the intimate binding of bone and titanium oxides (TiOx), a process known as osseointegration. A thin proteoglycan (PG)-rich layer exists at the interface between bone and TiOx which covers the surface of dental implant made of pure titanium. Chondroitin-4-sulfate (C4S), which links PGs, is generated by chondroitin-4-sulfate transferase-1 (C4ST-1) and binds directly to TiOx. To analyze the function of PGs on TiOx, human bone marrow mesenchymal stem cells (hBMSCs) depleted of C4ST-1 expression were analyzed *in vitro*. This study revealed that C4ST-1 controlled the width of the PG-rich layer between hBMSCs and TiOx. Moreover, C4ST-1 affected the immunotolerance, but not the osteogenic properties of hBMSCs on TiOx, suggesting a role of PGs in immunotolerance following implantation.

1. Introduction

Titanium (Ti) implants are widely used for prosthetic treatment due to the biocompatibility, mechanical characteristics, and corrosion resistance of Ti [1]. Osseointegration, the establishment of a direct connection between the anchoring element and living bone, is necessary for successful implant treatment, and is usually assessed under the microscope. However, the mechanisms underlying the osteogenic capacity and biocompatibility of Ti with bone, or the molecular interactions that occur at an implant interface are yet to be fully elucidated. Ultrastructural analysis of the interface between a Ti surface and bone has revealed the presence of a proteoglycan (PG)-rich layer ground substance at the intimate contact points between the implant surfaces and the adjacent bone [2–5]. Further studies have attempted to resolve the chemical composition of Ti-based dental implants in the human jaw at an atomic level, using TEM imaging with atom probe tomography [6].

For biochemical analysis of the PG-rich layer, PGs such as decorin, biglycan, and matrix gla protein, were immobilized onto Ti surfaces, and were found to play roles in calcification *in vitro* [7,8]. A PG unit consists of a core protein with one or more covalently

* Corresponding author.
E-mail address: t-shuhei@med.nagoya-u.ac.jp (S. Tsuchiya).

https://doi.org/10.1016/j.actbio.2020.07.034
1742-7061/

attached glycosaminoglycan (GAG) chains, and is categorized by its relative size (large or small) and the nature of its glycosaminoglycan chains [9]. Of the four groups investigated—heparan sulfate, chondroitin sulfate (CS)/dermatan sulfate (DS), keratan sulfate, and hyaluronic acid—chondroitin-4-sulfate (C4S) was the only glycosaminoglycan chain which demonstrated significant adsorption onto Ti in the presence of calcium ions [10]. GAGs were shown to play a role in establishing the mineralized tissue–titanium interfacial adhesion in the GAG/PG complex [11]. The structure of the PG-rich layer has been hypothesized to consist of C4S located on GAGs in the terminal region of PGs bound to the titanium oxide (TiOx) layer covering the surface of pure Ti materials [12,13]. Osseointegration requires moderate thickness of the PG-rich layer, whereas generation of the PG-rich layer requires adequate C4S on TiOx. Therefore, CS was utilized for surface modification of Ti implants in long bones [14].

Sulfation of the chondroitin backbone is mediated by the "4-O-sulfation" or "6-O-sulfation" pathways. The 4-O-sulfation of N-Acetylgalactosamine residues is found in high frequency in CS/DS chains [15]. Four phylogenetically related sulfotransferases that catalyze 4-O-sulfation have been cloned and characterized in mammals [16–20]. Among them, chondroitin 4-O-sulfotransferase-1 (C4ST-1), C4ST-2, and C4ST-3 preferably catalyze 4-O-sulfation of *N*-Acetylgalactosamine residues in CS. In the C4ST family, C4ST-1 plays a crucial role in skeletal development and signaling, and recent evidence suggests a potential role for C4ST-1 in human diseases, including cancer [21].

Various studies have discussed the interactions of bone marrow mesenchymal stem cells (BMSCs) with Ti and shown osteogenic properties, cell adhesion, and proliferation. However, BMSCs have an immunotolerance capacity, and can alter the tissue microenvironment via secretion of soluble factors by macrophages (Mps) [22,23]. Two Mp phenotypes have been established: the classical pro-inflammatory M1 and the alternative anti-inflammatory, wound healing M2 [24,25]. Implanted Ti has been shown to control inflammation caused by bacterial infection and foreign body reaction after surgical implantation. However, there have been no reports about direct and indirect effects on immunotolerance of BMSCs on Ti surfaces.

We hypothesized that C4ST-1 may regulate the formation of the PG-rich layer and affect the osteogenic properties and biocompatibility of human BMSCs (hBMSCs). To test our hypothesis, in the present study, we analyzed the function of C4ST-1 in hBMSCs on Ti surfaces.

2. Materials and methods

2.1. Cell culture

The human MSC cell line UE7T-13 was obtained from the Japanese Collection of Research Biosources (JCRB; Osaka, Japan). Cells were cultured in Dulbecco's Modified Eagle's medium (DMEM) containing 10% fetal bovine serum (FBS) (Sigma-Aldrich, Tokyo, Japan) and 1% penicillin and streptomycin (Fujifilm-Wako, Osaka, Japan) at 37 °C and 5% CO_2 under humidified conditions. THP-1 monocytes were purchased from JCRB and cultured in Roswell Park Memorial Institute (RPMI) 1640 medium containing 10% FBS and 1% PS. Preparation of the monocyte-Mps (hMps) transition was conducted according to a previous study [26].

2.2. Fabrication of Ti samples and characterization of surfaces

Pure Ti plates were obtained from Ofa Co., Ltd (Chiba, Japan), and Ti foil was obtained from Nirako (Tokyo, Japan). Ti plates were coated with 4.0 mM HNO_3 and 0.8 mM HF, then washed ultrasonically in 1% (w/v) sodium dodecyl sulfate (SDS) (Fujifilm-Wako), acetone (Fujifilm-Wako), and 70% ethanol, for subsequent use. The topography of the prepared Ti plates was observed using high-resolution scanning electron microscopy (SEM, JSM-7610F, JEOL Ltd, Tokyo, Japan). Electron-dispersive spectroscopy (EDS) analysis was carried out after the treatment to evaluate the chemical composition of the Ti surface.

2.3. Generation of stable cell lines

Custom-designed C4ST-1 shRNA, sh non-target control (SNC) (Takara Bio Inc., Shiga, Japan), pBA-HU6-puro plasmid vector (Takara Bio Inc.), restriction enzymes (Bam HI and Hind III; Takara Bio Inc.), and Mighty Mix (Takara Bio Inc.) were used for the sh-plasmids, which were transfected into UE7T-13 cells using ViaFect Transfection Reagent (Promega KK, Tokyo, Japan), according to manufacturer's protocols. After 24 h post-transfection, cells were selected using 0.1 μg/mL of puromycin (Sigma-Aldrich) for two weeks. Puromycin-resistant single clones were isolated, and eight independent clone lines were successfully established. The efficiency of depletion was determined by real-time RT-PCR and western blot analysis. The most efficient shRNA was chosen to deplete C4ST-1 throughout the study (sh-BMSCs). The non-target control was transfected using the same methods (N-BMSCs).

2.4. Real-time RT-PCR

Cells were seeded on the Ti plates at a density of $5 \times 10^2/cm^2$ and cultured for seven and 14 days. Total RNA was isolated using TRIzol LS Reagent (Thermo Fisher Scientific, Waltham, MA, USA), and cDNA was synthesized using ReverTra Ace qPCR RT Master Mix and gDNA Remover (Toyobo Co., Ltd., Osaka, Japan) according to the manufacturer's protocols. Quantitative real-time RT-PCR was performed using THUNDERBIRD SYBR qPCR Mix (Toyobo) and the Mx3000P Real-Time QPCR System (Agilent Technologies International Japan, Ltd., Tokyo, Japan). The expression of target transcripts was normalized against the expression of glyceraldehyde-3-phosphate dehydrogenase *(GAPDH)*, and relative changes in gene expression were determined using the $2^{-\Delta\Delta Ct}$ method. The primers are listed in Table 1.

2.5. Western blotting

Cells were fixed with 10% trichloroacetic acid for 30 min at 4 °C and harvested with a scraper. After centrifugation at 1000 × *g* for 5 min, the protein was diluted with a solution containing 2 M thiourea (Fujifilm-Wako), 7 M urea, 3% (w/v) CHAPS (Fujifilm-Wako), and 1% (w/v) triton X-100 (Fujifilm-Wako). Protein samples were mixed with 4 × sample buffer solution with 5% 2-mercaptoethanol (Fujifilm-Wako). Samples were separated by SDS-PAGE and transferred onto a PVDF membrane. After blocking with 5% Nonfat Dry Milk (Cell Signaling Technology, Tokyo, Japan) in Tween-PBS, each membrane was incubated with anti-GAPDH (1:10,000; ab181602; Abcam, Cambridge, United Kingdom) or anti-C4ST-1 (1:1000; PA5–68,129; Thermo Fisher Scientific) for 12 h at 4 °C. The membrane was incubated with Anti-Rabbit IgG, HRP-Linked Whole Ab (from donkey) (1:10,000, NA934V; GE Healthcare, Tokyo, Japan) as the secondary antibody for 1 h at room temperature. Antibody reactions were detected using an ECL Prime Western Blotting Reagent (GE Healthcare) and LuminoGraph I system (ATTO Corp., Tokyo, Japan).

2.6. Flow cytometry

Cells were suspended in Stain Buffer (FBS) (BD Biosciences, San Jose CA, USA) and incubated with CD14-PE-Cy7 (Clone 61D3),

Table 1
List of primers.

Gene	Sequence 5′–3′	3′–5′	Accession number of reference
C4ST-1	CATCAGGTTGGTGTGATGCAG	ACCATGCACAGCACACATTG	NM_001173982.1
C4ST-2	TCGGTGTTCATGATCCTGCTG	AGAGAAGGACGTGTGCAAGTAG	NM_001243794.1
C4ST-3	CGTAGATGGGCAAGGACTTG	ACACCGGTGTCAGCATTATG	NM_152,889.2
IL-6	AATGAGGAGACTTGCCTGGTG	TGTACTCATCTGCACAGCTCTG	NM_000600.4
IL-10	ATCAAGGCGCATGTGAACTC	AAGGCATTCTTCACCTGCTC	NM_000572.3
IDO	TCCTTACTGCCAACTCTCCAAG	CGTCCATGTTCTCATAAGTCAGG	AH002828.2
CD80	GTTATCCACGTGACCAAGGAAG	TTGTGCCAGCTCTTCAACAG	NM_005191.4
CD86	ACTGTACGACGTTTCCATCAGC	AGCCGCGTCTTGTCAGTTTC	KU284848.1
CD163	AAGACGCTGCAGTGAATTGC	AATGGCCAACAGAACAACCC	DQ058615.1
CD206	TGGAGCAGGTGGAAGATCTATG	ACTTGAACGGGAATGCACAG	NM_002438.4
Runx2	AAGCTTGATGACTCTAAACC	TCTGTAATCTGACTCTGTCC	NM_001024630.3
OCN	CACACTCCTCGCCCTATTGG	CGCCTGGGTCTCTTCACTAC	NM_199,173.6
Col1	GCTATGATGAGAAATCAACCG	TCATCTCCATTCTTTCCAGG	NM_000088.3
GAPDH	AGCAAGAGCACAAGAGGAAGAG	TCTACATGGCAACTGTGAGGAG	NM_001289745.2

Abbreviations: C4ST; Chondroitin 4-Sulfotransferase, Runx2; Runt-related transcription factor 2, ALP; Alkaline phosphatase, IDO; Indoleamine-pyrrole 2,3-dioxygenase, GAPDH; glyceraldehyde-3-phosphate dehydrogenase.

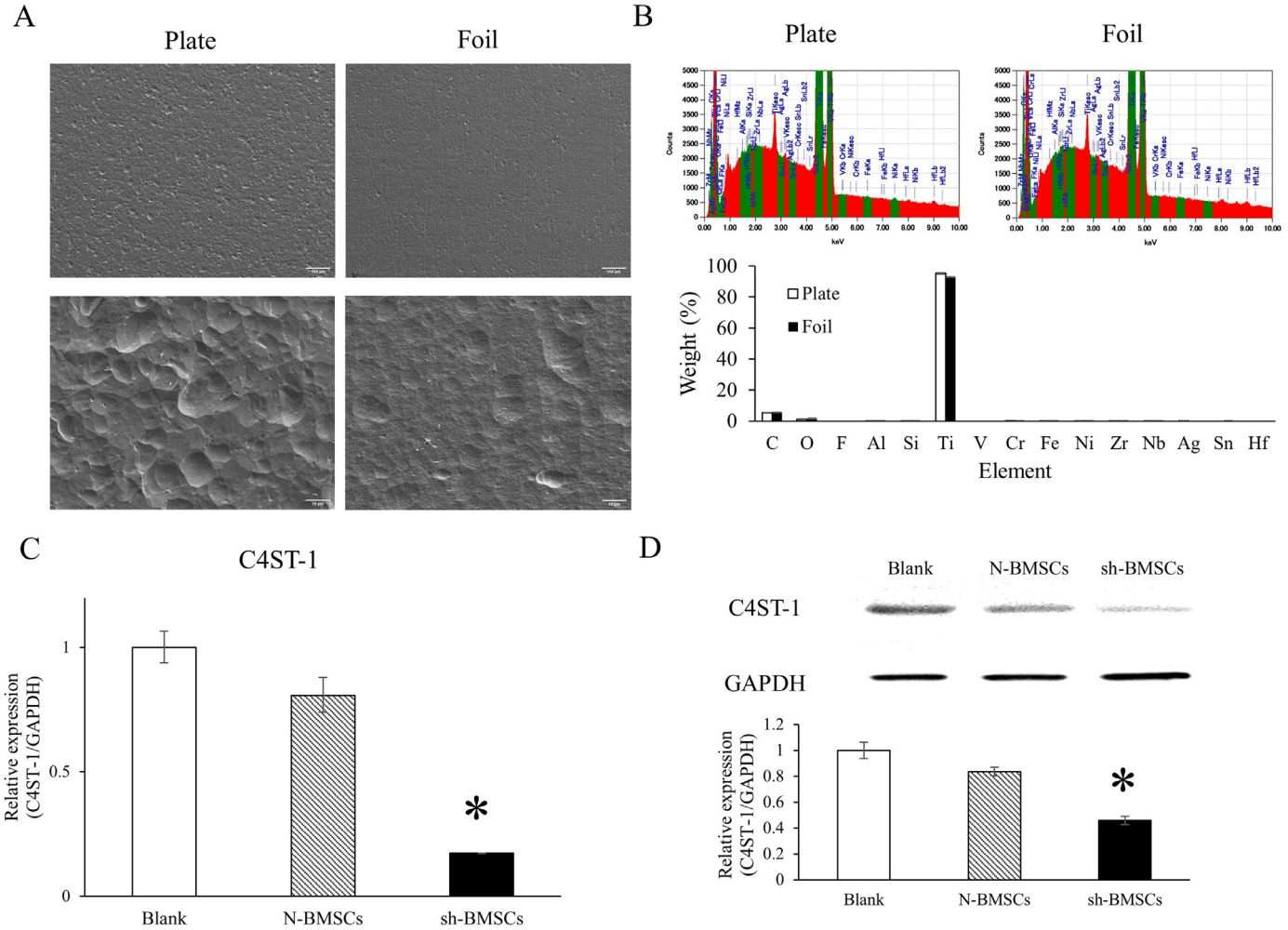

Fig. 1. SEM micrographs showing surface roughness of tested Ti plate and foil. (A) SEM images at 100 × and 1000 × magnification. (B) SEM-EDX analysis of Ti surface. The composition of elements on Ti plate. The composition of elements on Ti foil. The comparison of quantitative elemental distribution between Ti plate and foil. The numbers on the EDX spectra represent mean weight (w)%. The abbreviations are: C; carbon, O; oxygen, F; fluorine, Al; aluminum, Si; silicon, Ti; titanium, V; vanadium, Cr; chromium, Fe; iron, Ni; nickel, Zr; zirconium, Nb; niobium, Ag; silver, Sn; Tin, Hf; hafnium. To measure C4ST-1 shRNA expression, UE7T-13 cells were transfected with the pBA-HU6-puro plasmid harboring shRNA targeting C4ST-1. (C) mRNA and (D) protein expression analysis of C4ST-1. Three samples were prepared and measured three times each. Nine analyses were performed in total. * $p < 0.05$ vs. blank and N-BMSCs.

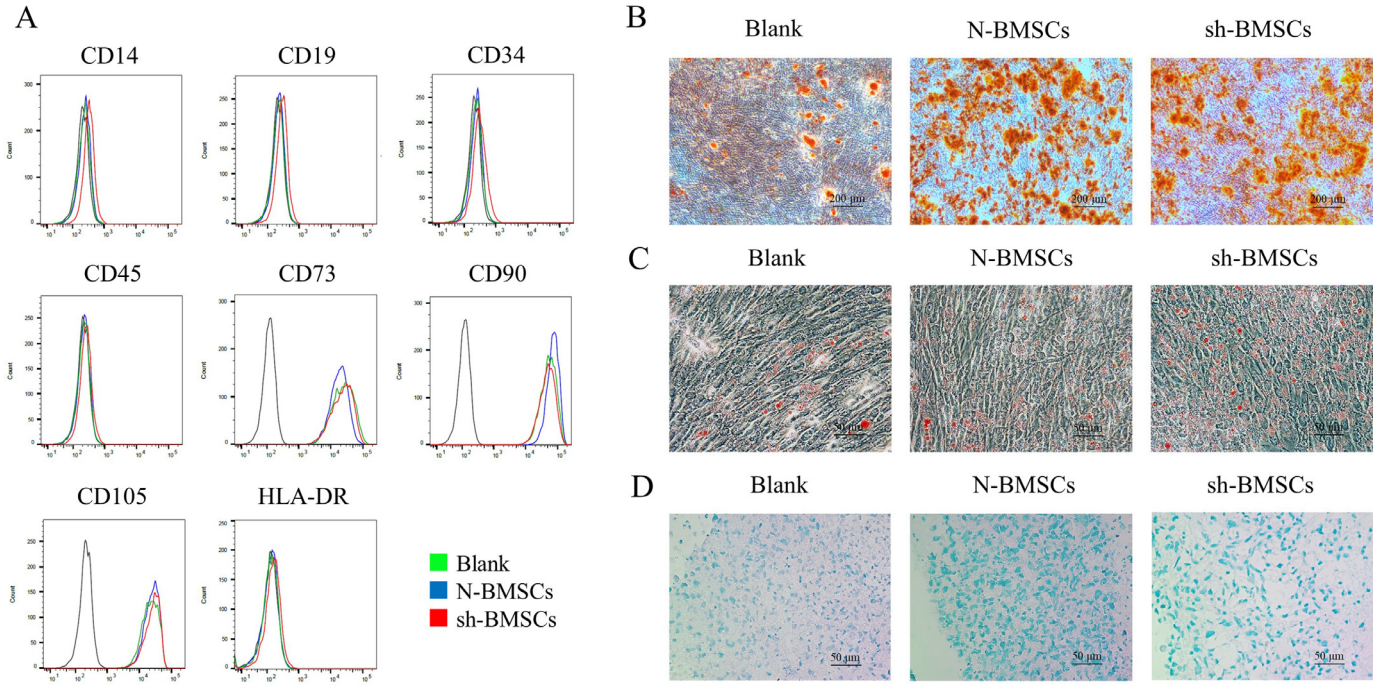

Fig. 2. Characterization and trilineage differentiation capacity of UE7T-13, N-BMSCs, and sh-BMSCs. (A) Representative flow cytometry analysis of cell surface markers. (B) Alizarin Red S staining of mineralized extracellular matrix after osteogenic differentiation. (C) Oil Red O staining for intracellular lipid vesicles during adipogenic differentiation. (D) Alcian Blue staining of chondrogenic differentiation. Three samples were prepared and measured three times each. Nine analyses were performed in total. The bar represents 50 μm. (For interpretation of the references to colour in this figure legend, the reader is referred to the web version of this article.)

Table 2
Analysis of components on Ti plate and foil by SEM-EDX.

% element by weight (wt%) (mean ± SEM)	Plate	Foil
C	3.31 ± 0.07	5.55 ± 0.15
O	1.05 ± 0.26	1.52 ± 0.32
F	0 ± 0	0 ± 0
Al	0.02 ± 0.01	0.01 ± 0.01
Si	0.03 ± 0	0.02 ± 0.
Ti	95.2 ± 0.4	92.7 ± 0.15
V	0 ± 0	0 ± 0
Cr	0.00 ± 0	0.02 ± 0.01
Fe	0.04 ± 0.02	0.02 ± 0.01
Ni	0.14 ± 0.02	0.02
Zr	0.04 ± 0.03	0.01 ± 0.01
Nb	0.01 ± 0.01	0 ± 0.01
Ag	0.04 ± 0.01	0 ± 0
Sn	0 ± 0	0.01 ± 0.01
Hf	0 ± 0	0 ± 0

CD19-PE-Cy7 (Clone SN6), CD34-PE-Cy7 (Clone 4H11), CD45-PE-Cy7 (Clone HI30), CD73-APC (Clone AD2), CD90-APC (Clone 5E10), CD105-PE-Cy7 (Clone SN6), and HLA-DR-Alexa Fluor 700 (Clone LN3) for 30 min on ice. All antibodies were purchased from Thermo Fisher Scientific. Stained cells were analyzed using the FACS Canto II system (Becton, Dickinson and Company, Tokyo, Japan).

2.7. Cell proliferation assay

The Ti foil was punched out to make thin circular plates, 6 mm in diameter, which were placed in 96-well plates. After seeding 1×10^2 cells on Ti plates for 24, 48, and 72 h, proliferation assays were carried out using Cell Counting Kit-8 (Dojindo Laboratories, Kumamoto, Japan) in accordance with the manufacturer's instructions. Absorbance was determined using the Infinite 200 PRO system and i-control software (Tecan Japan Co., Ltd., Kanagawa, Japan).

2.8. Alizarin red s staining

For staining, 2×10^4 cells were seeded on the Ti plates (30 mm in diameter) and cultured with DMEM supplemented with 50 μg/mL ascorbic acid, 100 nM dexamethasone, and 10 mM β-glycerophosphate for 7 and 14 days. Each plate was fixed with 10% formalin and stained with 1% alizarin red S solution (Fujifilm-Wako) for 10 min at room temperature. After staining, the cells were washed five times with distilled water. The dye was then dissolved using 500 μL of 5% formic acid for 20 min, and absorbance was measured at 415 nm OD using the Infinite 200 PRO system (Tecan Japan Co., Ltd.).

2.9. Immunocytochemical (ICC) analysis

Cells were seeded on the Ti plates at a density of $1 \times 10^2/cm^2$ and cultured for 1 and 3 h. The cells were fixed with 4% paraformaldehyde for 15 min at room temperature, then permeabilized with 0.2% triton X-100 in PBS for 20 min. After blocking using Blocking One Histo (Nacalai Tesque, Inc., Kyoto, Japan) for 10 min, each plate was incubated with anti-vinculin (1: 250; ab129002; Abcam) for 14 h at 4 °C, then incubated with Goat anti-Rabbit IgG (H+L) Highly Cross-Adsorbed Secondary Antibody, Alexa Fluor 546 (4 μg/mL; A11035; Thermo Fisher Scientific) for 1 h and Actin-stain 488 phalloidin (100 nM, Cytoskeleton, Inc. Co, Denver CO, USA) for 1 h in the dark. Finally, each plate was mounted with DAPI (Vector Laboratories, Inc., Burlingame, CA, USA) and observed using the BZ-X810 All-in-One Fluorescence Microscope (Keyence, Osaka, Japan). Image analysis was performed using ImageJ (https://imagej.net/Welcome; National Institutes of Health, Bethesda, MD,

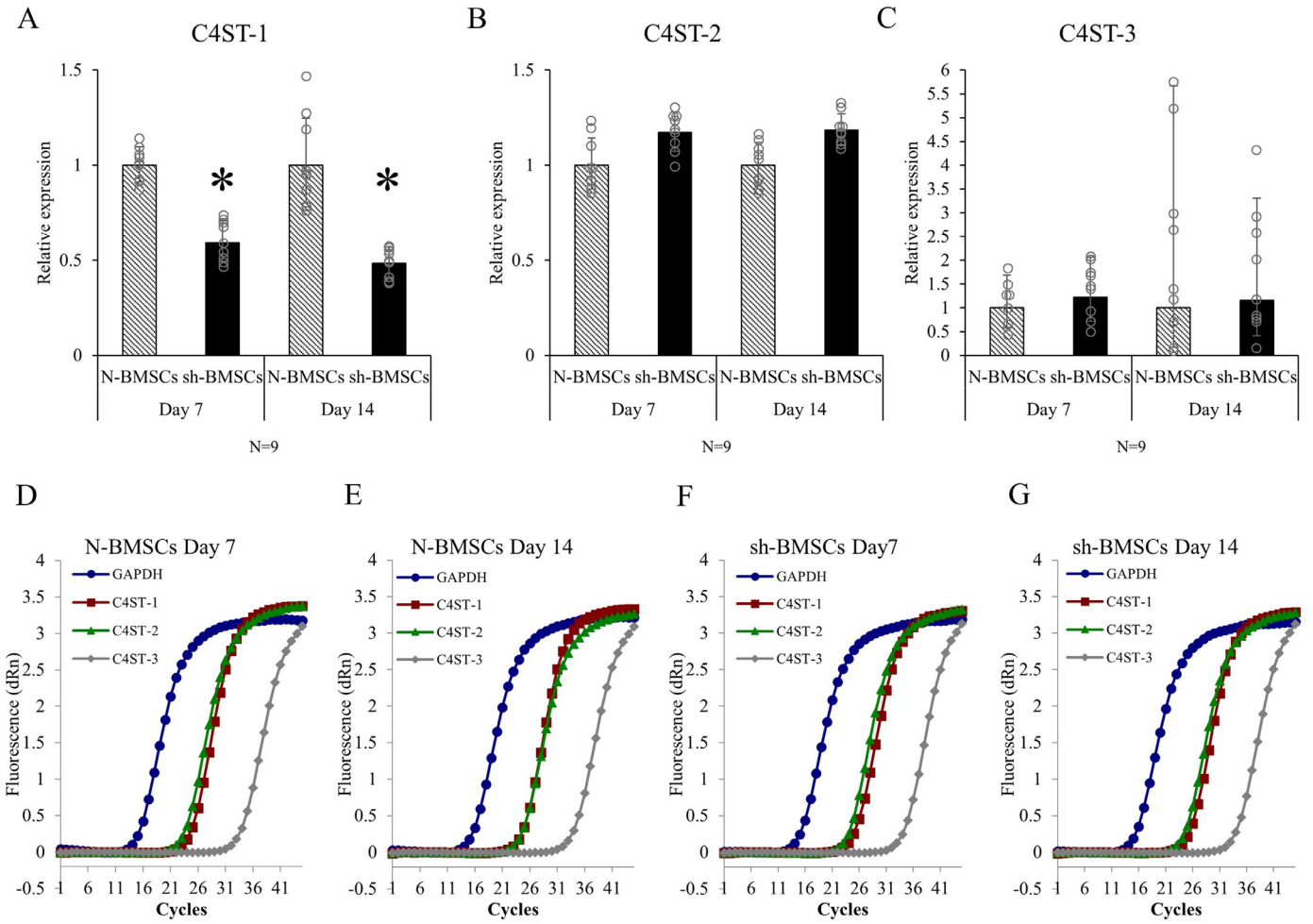

Fig. 3. Gene expression level of C4ST-1, -2, -3 in N-BMSCs and sh-BMSCs on TiOx by real time RT-PCR. Expression of (A) C4ST-1, (B) C4ST-2, and (C) C4ST-3 in N-BMSCs and sh-BMSCs on TiOx at 7- and 14-day cultivation. Amplification plot of GAPDH, C4ST-1, -2, and -3 in N-BMSCs at (D) 7 days and (E) 14 days cultivation on TiOx. Amplification plot of GAPDH, C4ST-1, -2, and -3 in sh-BMSCs at (F) 7 days and (G) 14 days cultivation on TiOx. Three samples were prepared and measured three times each. Nine analyses were performed. * $p < 0.05$ vs. N-BMSCs. (For interpretation of the references to colour in this figure legend, the reader is referred to the web version of this article.)

Table 3
Analysis of surface markers expression by flow cytometry.

	Percent of cells with expression markers (mean ± SEM)							
	CD14	CD19	CD34	CD45	CD73	CD90	CD105	HLA-DR
Blank	0 ± 0	0.01 ± 0.009	0.03 ± 0.040	0 ± 0	100.0 ± 0.058	99.9 ± 0.100	99.0 ± 0.058	0.02 ± 0.011
N-BMSCs	0.01 ± 0.009	0 ± 0	0.006 ± 0.010	0.01 ± 0.009	99.8 ± 0.058	99.7 ± 0.100	96.9 ± 0.265	0 ± 0
sh-BMSCs	0.02 ± 0.016	0 ± 0	0.01 ± 0.018	0 ± 0	99.9 ± 0.100	99.8 ± 0.058	98.5 ± 0.153	0.01 ± 0.009

USA). Images of vinculin staining were thresholded to identify adhesion complexes.

2.10. Transmission electron microscopy

For transmission electron microscopy, $5 \times 10^2/cm^2$ cells were seeded on the Ti foil discs of 6 mm diameter. After 7 and 14 days of cultivation, samples were washed three times with 0.1 M sodium cacodylate buffer, fixed with a pre-fixative containing 4% paraformaldehyde, 2% glutaraldehyde, and 0.1 M sodium cacodylate for 1 h at 4 °C, and immersed in 0.05% ruthenium red solution for 1 h at room temperature; ruthenium red is a polycationic dye that has been used to stain negatively charged molecular species in tissue sections. A post-fixative containing 1% OsO_4 and 0.05% ruthenium red was then applied for 1 h at room temperature, followed by dehydration with ethanol and embedding in EPON resin (Nisshin EM Co., Ltd., Tokyo, Japan). After curing, part of the foil was physically removed, and the samples were re-embedded in EPON resin. These samples were cut with an ultramicrotome (EM UC7i, Leica, Tokyo, Japan), stained with lead citrate for 5 s, and observed with a transmission electron microscope (JEM-1400PLUS, JEOL).

2.11. Immunotolerance assay of BMSCs and hMps

N-BMSCs and sh-BMSCs were cultured on 30 mm Ti plates for 14 days. The medium was changed to DMEM without FBS for 24 h to prepare the conditioned medium (CM). CM was then added to hMps and cultured for 24 h. Total RNA was extracted to analyze the macrophage polarization.

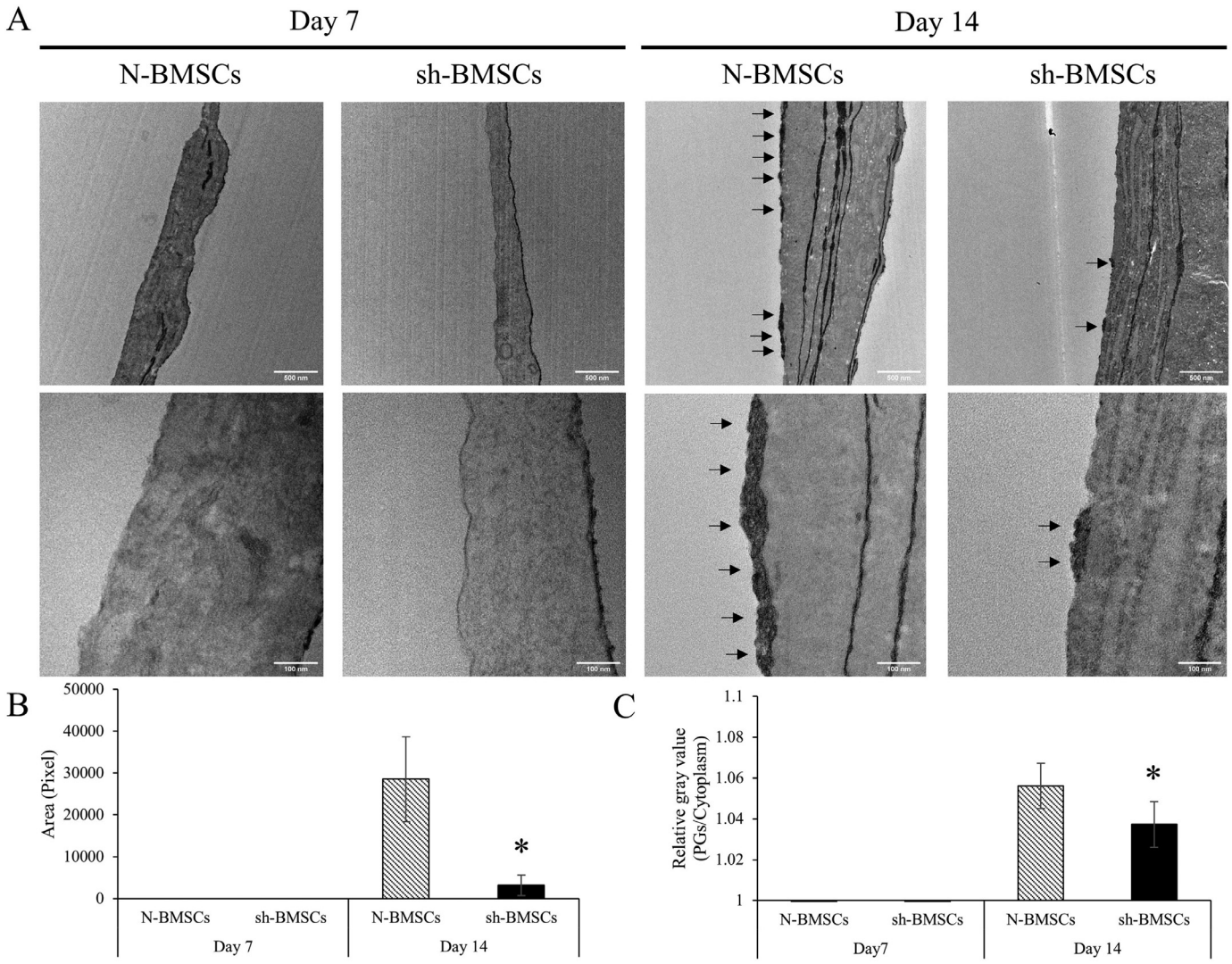

Fig. 4. PG-rich layer formation *in vitro*. (A) Electron micrograph of the cell–TiOx interface. The PG-rich layer is interposed between the TiOx and N-BMSCs and sh-BMSCs (arrows) at 14 days cultivation. Quantification of the PG-rich layer based on (B) pixel or (C) relative gray value (PG-rich layer / cytoplasm). The bar represents 500 nm (Upper) and 100 nm (Lower), respectively. Three samples were prepared each experimental group, and fifteen images in total for N-BMSCs and sh-BMSCs were analyzed. * $p < 0.05$ vs. N-BMSCs.

2.12. Image and statistical analyses

ICC and TEM images were analyzed using ImageJ software (NIH). All experiments were carried out in triplicate, and data are expressed as mean ± standard deviation. Statistical significance was analyzed using a non-parametric test, and results with $p < 0.05$ were considered statistically significant.

3. Results

3.1. Topology of the Ti plates

SEM images of the Ti plates and foil showed typical smooth surfaces without parallel grooves or microstructure, indicating that the treatment methods removed surface contamination (Fig. 1A). SEM-EDX analysis showed that the amount of Ti on the surface of the Ti plates was not significantly different from that of Ti foil. The amount of Al and V was not significantly different between Ti plate and foil. The amount of Al on Ti plate and foil was measured as 0–0.02%. No V was detected on the Ti plate or foil (Fig. 1B and Table. 2).

3.2. Characterization of sh-BMSCs

In the sh-BMSCs, C4ST-1 mRNA levels were significantly decreased, to approximately 17%, compared to two control cells (Fig. 1C). C4ST-1 protein levels in the sh-BMSCs were significantly decreased to about 45.9%, compared to control cells (Fig. 1D). No expression of CD14, CD19, CD34, CD45, and HLA-DR was detected in either the sh-BMSCs or the N-BMSCs. In contrast, CD73, CD90, and CD105 expression was detected in the sh-BMSCs and N-BMSCs. The number of cells detected was not significantly different between sh-BMSCs and N-BMSCs (Fig. 2A). The expression patterns of the stem cell markers are summarized in Table 3. A multipotency assessment of BMSCs, N-BMSCs, and sh-BMSCs was performed, and indicated that all groups had osteogenic- (Fig. 2B), adipogenic- (Fig. 2C), and chondrogenic-differentiation (Fig. 2D) capacities.

3.3. Expression of C4ST-1, -2, and -3 in sh-BMSCs and N-BMSCs on TiOx

The expression patterns of C4ST-1, -2, and -3 in sh-BMSCs and N-BMSCs on TiOx were analyzed. The expression of C4ST-1 in sh-

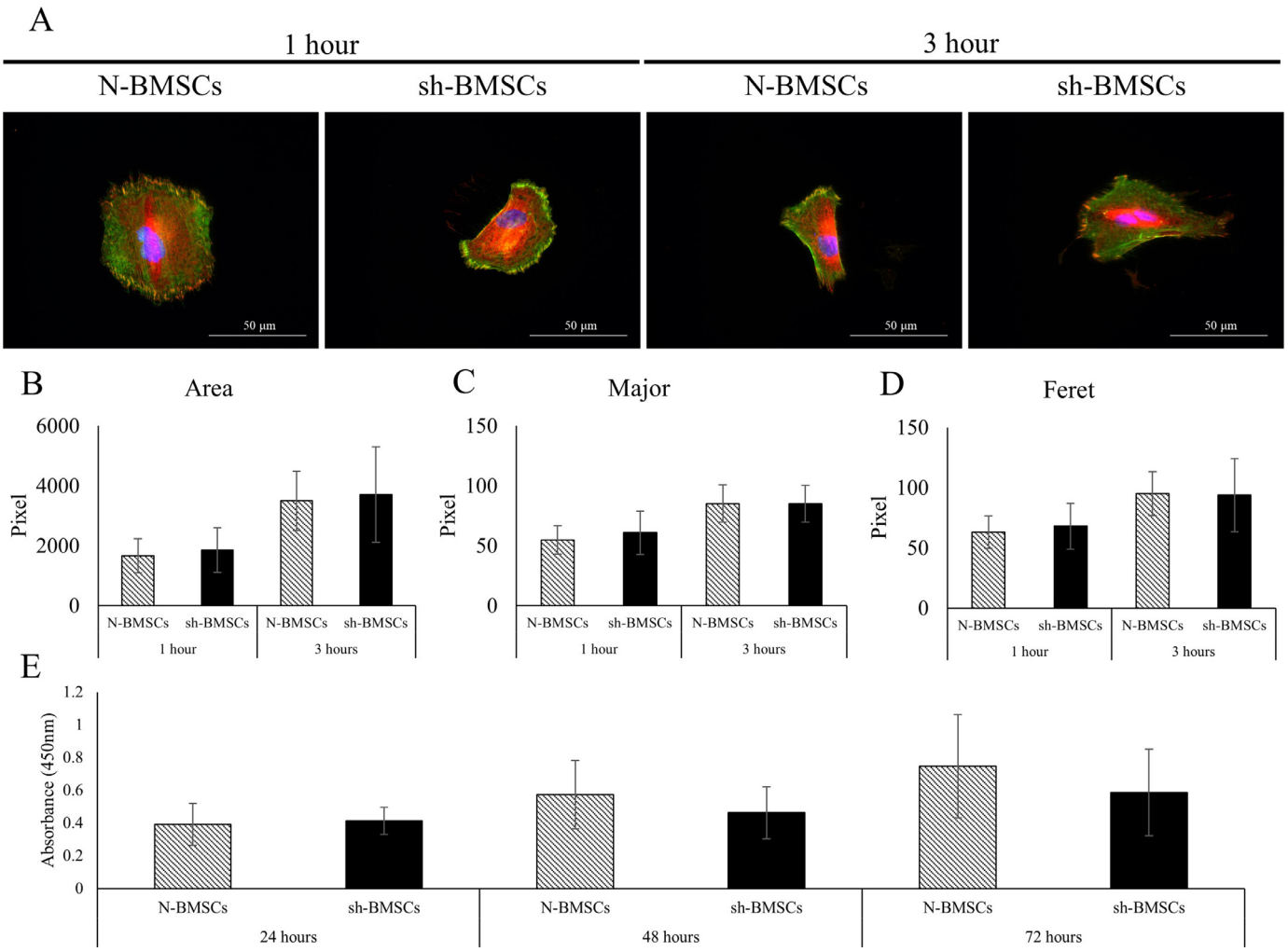

Fig. 5. Initial cell adhesion and cell proliferation of N-BMSCs and sh-BMSCs on TiOx. (A) Expression of vinculin in N-BMSCs and sh-BMSCs on TiOx. Green: f-actin, Red: vinculin, Blue: DAPI. Quantification of focal adhesion based on (B) area, (C) major, or (D) feret. (E) Cell proliferation of N-BMSCs and sh-BMSCs on TiOx at 24, 28, and 72 h. The figure is representative of three independent experiments. At least fifteen cells were analyzed, and cells contacting other cells were excluded. NC 1 h: $N = 30$, sh 1 h: $N = 31$, NC 3 h: $N = 16$, sh 3 h: $N = 20$. * $p < 0.05$ vs. N-BMSCs. (For interpretation of the references to colour in this figure legend, the reader is referred to the web version of this article.)

BMSCs on TiOx was significantly decreased by 43.1% at 7 days, and by 36.9% at 14 days after cultivation compared to N-BMSCs on TiOx (Fig. 3A). However, the expression of C4ST-2 and -3 in sh-BMSCs on TiOx was not significantly different than that of N-BMSCs on TiOx (Fig. 3B, 3C). Amplification plots showed that the expression of C4ST-3 was significantly lower than that of C4ST-1 and -2 at all time points, and among all experimental groups (Fig. 3D, E, F, and G).

3.4. *Effect of C4ST-1 on PG-rich layers in BMSCs on TiOx* in vitro

TEM imaging was used to examine the interface between BMSCs and the Ti plate. Ruthenium red staining indicated a PG-rich area, which indicated the PG-rich layer [27]. No PG-rich layer was observed between the cell membrane and TiOx after 7 days of culture in any experimental group. However, a PG-rich layer in N-BMSCs on TiOx was clearly observed compared to sh-BMSCs after 14 days of culture (Fig. 4A). N-BMSCs and sh-BMSCs formed a 80–100 nm wide PG-rich layer. After quantifying the ruthenium red-stained area in N-BMSCs and sh-BMSCs on TiOx at 14 days after culture, the area of the PG-rich layer in sh-BMSCs was found to be significantly lower than that of N-BMSCs (Fig. 4B). The relative gray value of the PG-rich layer/cytoplasm in sh-BMSCs on TiOx was significantly lower than that of N-BMSCs on TiOx (Fig. 4C).

3.5. *Effect of C4ST-1 on initial cell adhesion and cell proliferation in BMSCs on TiOx*

The initial cell adhesion of BMSCs to TiOx was analyzed by staining with vinculin and phalloidin at 1 and 3 h (Fig. 5A). The area stained with vinculin was around the nucleus in N-BMSCs and sh-BMSCs. However, quantification of the area (Fig. 5B), major (Fig. 5C), and feret diameter (maximum caliper, referring to the measurement of the object size with a caliper) (Fig. 5C) of sh-BMSCs on TiOx showed no significant differences compared to N-BMSCs at any time point. Proliferation of sh-BMSCs on TiOx appeared to be lower than that of N-BMSCs, but the difference was not statistically significant (Fig. 5E).

3.6. *Effect of C4ST-1 on osteogenic properties in BMSCs on TiOx*

The expression of osteogenic-related genes was analyzed using real-time RT-PCR (Fig. 6A, B, C, and D). At seven days after culture, the expression of Col1α1 in sh-BMSCs on TiOx was significantly lower than in N-BMSCs, whereas that of Runx2 was sig-

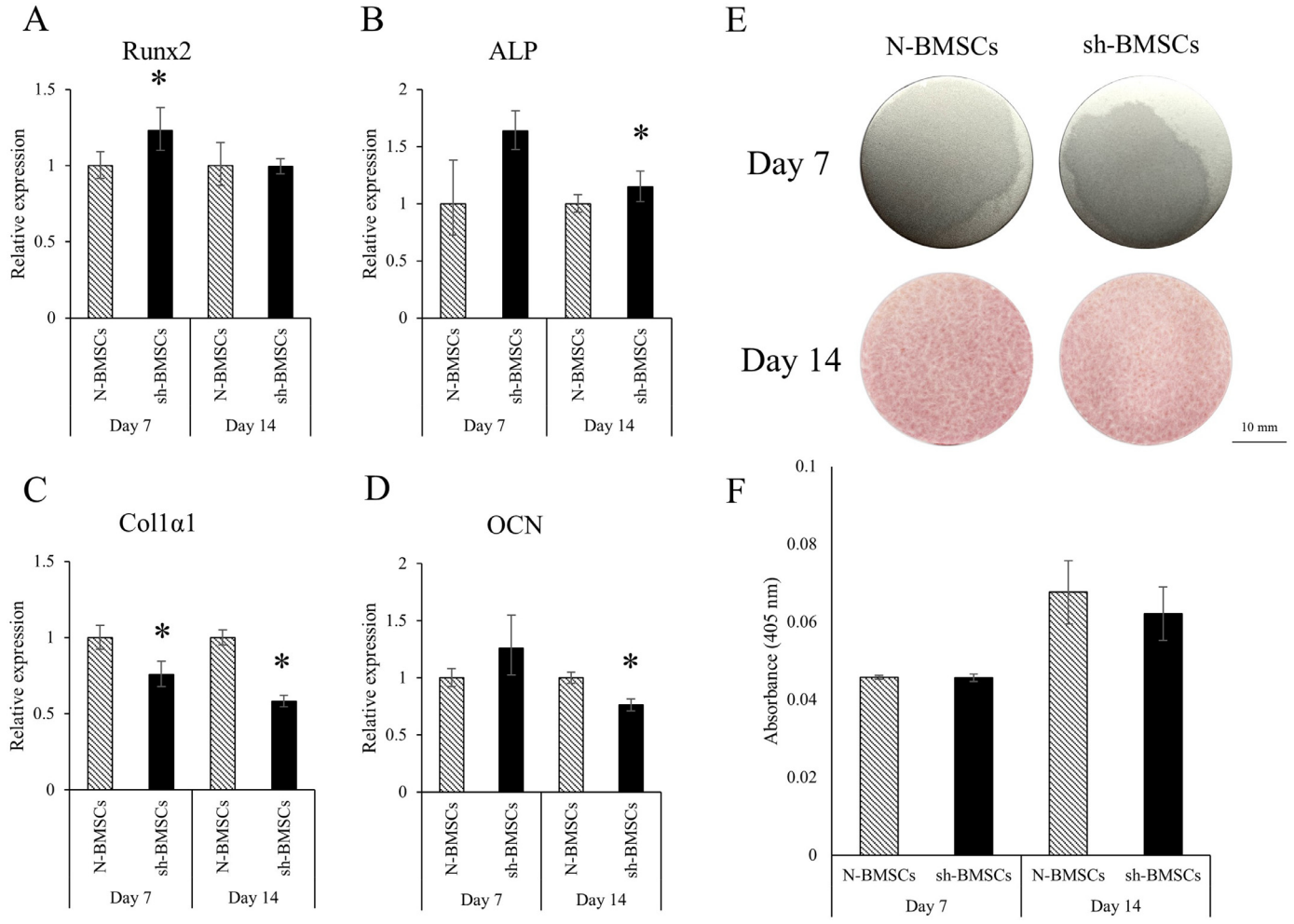

Fig. 6. Osteogenic capacity of N-BMSCs and sh-BMSCs on TiOx at 7- and 14-days cultivation. Gene expression of (A) Runx2, (B) ALP, (C) Col1α1, and (D) OCN in N-BMSCs and sh-BMSCs on TiOx. (E) Mineralized nodule formation in N-BMSCs and sh-BMSCs on TiOx by Alizarin red S staining (upper) and quantitative analysis (lower). The figure is representative of three independent experiments. * p <0.05 vs. N-BMSCs. (For interpretation of the references to colour in this figure legend, the reader is referred to the web version of this article.)

nificantly higher. Fourteen days after culture, the expression of Col1α1 and BGLAP in sh-BMSCs was significantly lower than that in N-BMSCs. ALP expression in sh-BMSCs was significantly higher than in N-BMSCs. Calcified nodules were formed in N-BMSCs and sh-BMSCs on TiOx, and their quantification showed no significant differences between N-BMSCs and sh-BMSCs at any time point (Fig. 6E).

3.7. Effect of C4ST-1 on immunotolerance in BMSCs on TiOx

Real-time RT-PCR was performed to analyze the effect of C4ST-1 on immunotolerance of BMSCs for TiOx. Expression levels of IL-6 and IDO in sh-BMSCs on TiOx were significantly higher than those in N-BMSCs on TiOx (Fig. 7A and C). However, there was no significant difference in IL-10 expression between N-BMSCs and sh-BMSCs on TiOx (Fig. 7B). CM derived from N-BMSCs and sh-BMSCs cultured on TiOx affected the differentiation of hMps. The expression of IL-6, CD80, and IDO, which are markers of M1 macrophages, was significantly higher in hMps treated with CM derived from sh-BMSCs than in N-BMSCs (Fig. 8A, B, and D). However, there was no significant difference in IL-10, CD86, CD163, and CD206 expression in hMps between N-BMSCs and sh-BMSCs treatments (Fig. 8C, E, F, and G).

4. Discussion

In this study we analyzed whether C4ST-1 in BMSCs affected the formation of a PG-rich layer on TiOx, and their osteogenic properties. We first characterized sh-BMSCs, in which C4ST-1 did not affect the stem cell phenotype. A previous report has shown that C4ST-1 did not influence cell proliferation, migration, or differentiation in neural stem cells [28]; sh-BMSCs retained the stem cell phenotype and could therefore be used for the cell differentiation assay on TiOx.

We then investigated the expression levels of C4ST-1, -2, and -3 in BMSCs cultured on TiOx. The behavior of sh-BMSCs could be observed for two weeks. Depletion of C4ST-1 in BMSCs did not affect C4ST-2 and -3 expression. Therefore, the effect of C4ST-1 in BMSCs on TiOx could be assessed using sh-BMSCs.

We used TEM to investigate whether C4ST-1 affected the morphology of the PG-rich layer formed by BMSCs on TiOx. In this study, depletion of C4ST-1 reduced the formation of the PG-rich layer. TEM imaging and expression analysis of C4ST family members suggested that C4ST-1 played the pivotal role in PG-rich layer formation. Multiple studies have reported that a PG-rich layer exists 20–500 nm from the implant surface [29,30,2,5,31]. The thickness of the PG-rich layer in this study was similar to those identified in previous studies and *in vivo* findings. Thus, this experi-

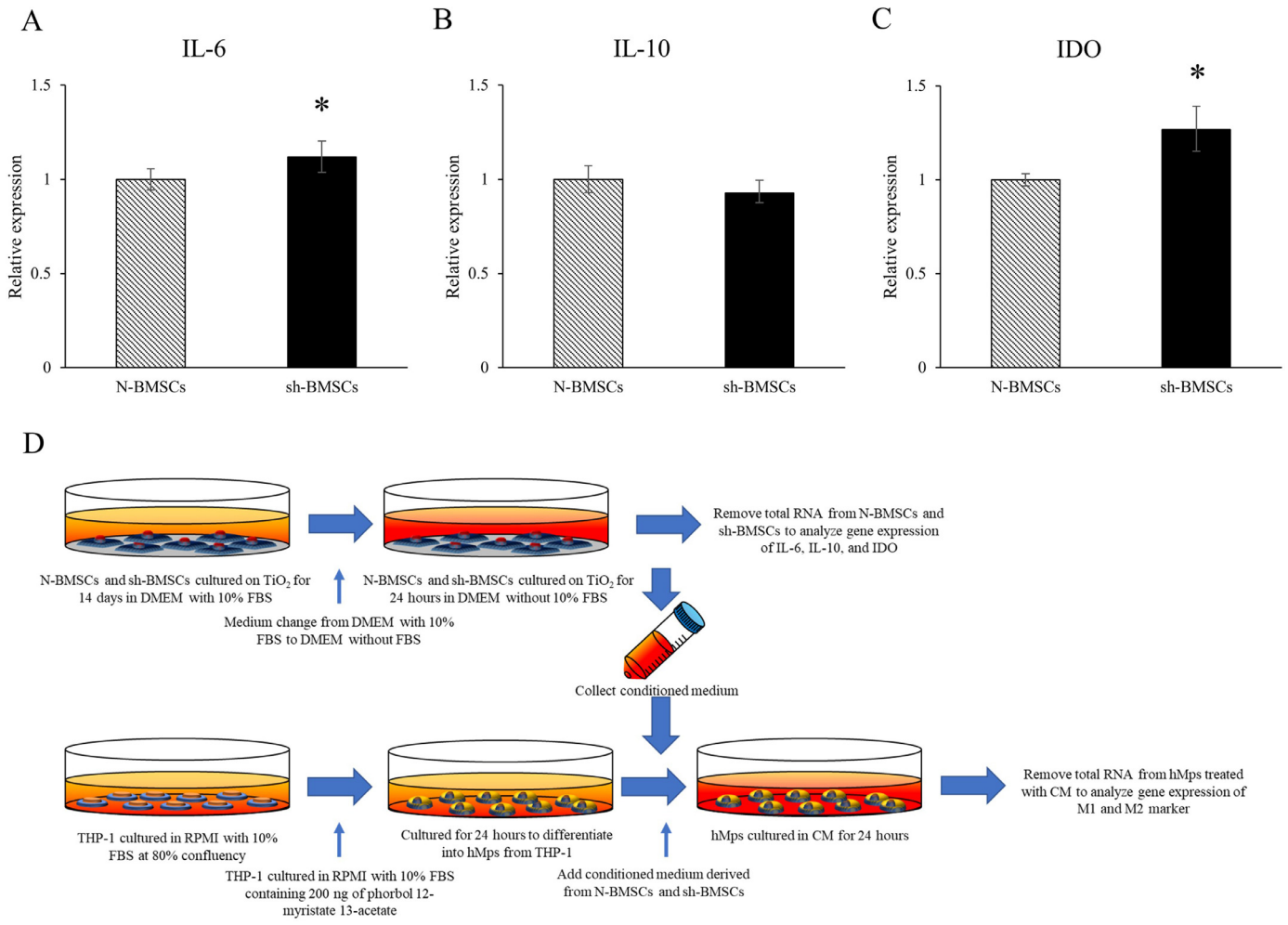

Fig. 7. Gene expression related to immunotolerance in N-BMSCs and sh-BMSCs on TiOx at 14 days cultivation. Expression of (A) IL-6, (B) IL-10, and (C) IDO in N-BMSCs and sh-BMSCs on TiOx. (D) Graphical materials and methods in the immunotolerance assay. The figures, except for (D), are representative of three independent experiments. Nine analyses were performed in total. * $p < 0.05$ vs. N-BMSCs.

mental procedure may be applicable to analyze the PG-rich layer in animals. Depletion of C4ST-1 did not affect the thickness of the PG-rich layer. A previous study identified a 30–60 nm-wide layer with low electron density, which contacted the Ti surface along a high electron density layer *in vivo* [32]. This low electron density layer was not observed in our study, suggesting that these differences impacted the surface topology of Ti and possibly altered the morphology of the PG-rich layer. Since, the Ti surface used by Okamatsu et al. [32] differed from that used in our study, TEM analysis of BMSCs cultured on different surface topologies of Ti should therefore be conducted in the future, to validate these findings.

C4ST-1 did not affect cell proliferation, adhesion, or osteogenic properties on TiOx. However, the presence of CS-A and CS-B in collagen fibrils coating Ti surfaces appeared to increase the formation of focal adhesions [33]. Previous reports have shown that proteoglycan degradation by exogenic treatment reduced mineralization on Ti surfaces *in vitro* and *in vivo* [11,8,34–36]. It was suggested that these differences were caused by differences in experimental design because the chondrocytes treated with endogenous growth factors showed differences in GAG and PG synthesis compared to those treated with exogenous growth factors [37,38]. We found that 10–30% difference in osteogenesis-related genes between N-BMSCs and sh-BMSCs did not affect the number of calcified nodules on TiOx. Another report showed that C4S did not promote osteogenic differentiation in BMSCs [39]. Taken together, these results suggested that the PG-rich layer did not affect the cell proliferation or osteogenic properties of hBMSCs on TiOx.

Depletion of C4ST-1 increased the immunotolerance of BMSCs for TiOx, and C4ST-1 depletion in BMSCs indirectly promoted polarization of M1-like macrophages from hMps. Together with the TEM analysis, these results suggested that the PG-rich layer inhibited the immunotolerance capacity of BMSCs on TiOx, and affected secretion from BMSCs on TiOx to stimulate differentiation of M0 macrophages to M2-like macrophages. CS has a heterogeneous structure due to the organization of multiple CS disaccharide sulfation motifs that give rise to a wide range of CS chain structures, and hence impart a wide range of biological activities [40]. However, to our knowledge, there have been no reports on whether GAG affects immunotolerance and secretion from BMSCs. Future studies should address the structures of the sugar chains derived from BMSCs on TiOx to analyze the effect of C4S on immunotolerance in BMSCs on TiOx.

Only smooth surfaces were investigated in this study. Other studies have reported that various types of rough surfaces produced by treatments such as anodic oxidation, acid etching, blasting, or both etching and blasting, enhance osseointegration. Numerous reports have shown that topological modifications affect the differentiation of BMSCs [41,42]. Therefore, in future work we will investigate whether surface topology affects the formation of the PG-rich layer, and compare these results with those of clini-

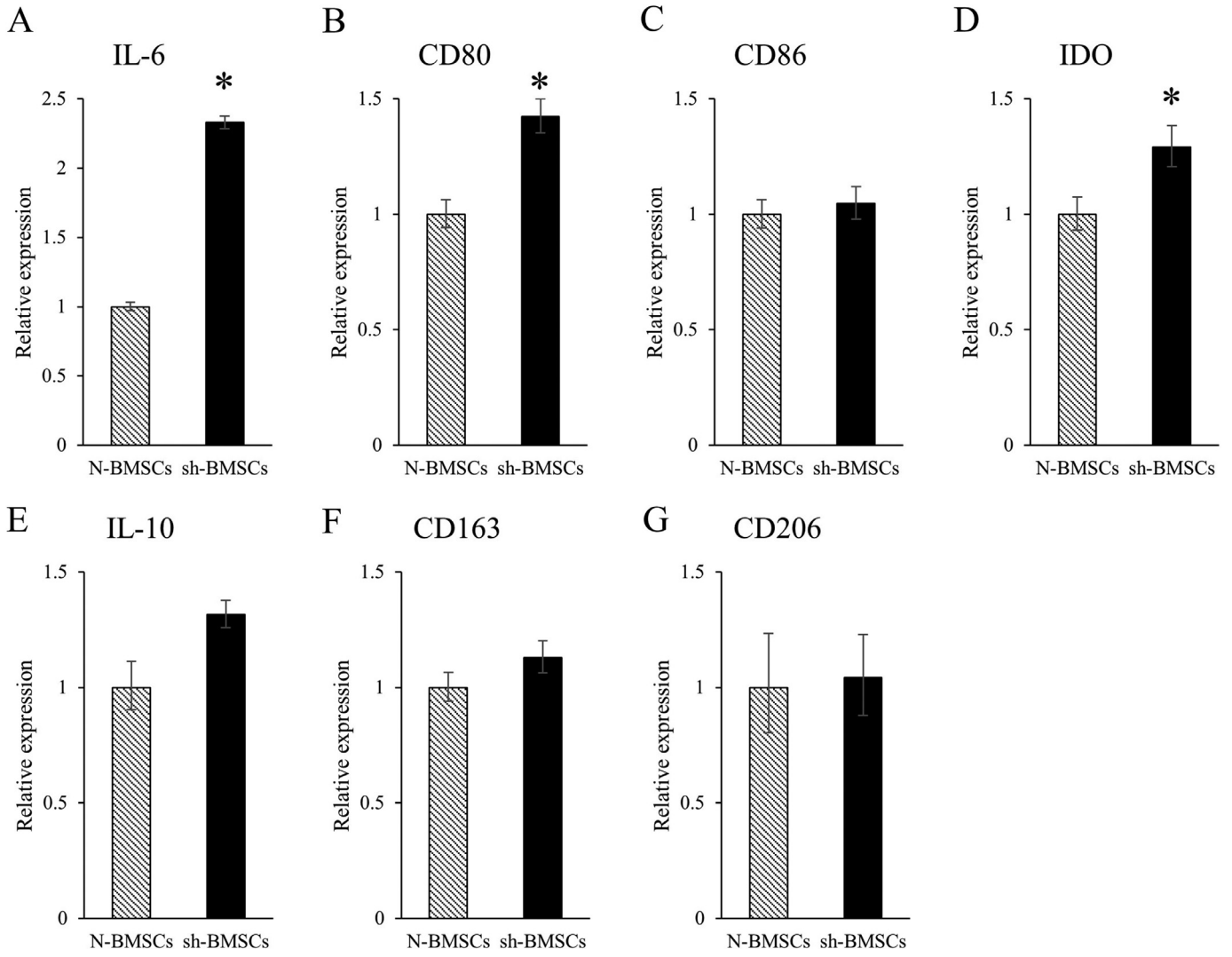

Fig. 8. Gene expression related to immunotolerance in CM-treated hMps derived from N-BMSCs and sh-BMSCs on TiOx at 14 days cultivation. Expression of (A) IL-6, (B) CD80, (C) CD86, (D) IDO, (E) IL-10, (F) CD163, and (G) CD206 in hMps. The figures are representative of three independent experiments. Nine analyses were performed in total. * $p < 0.05$ vs. N-BMSCs.

cal studies which have reported good results using various types of rough surfaces.

5. Conclusions

This study revealed that although C4ST-1 affected the PG-rich layer of BMSCs on TiOx, it did not influence cell proliferation or osteogenic differentiation. Furthermore, the PG-rich layer altered the immunotolerance of BMSCs on TiOx both directly and indirectly.

Declaration of Competing Interest

The authors declare that they have no known competing financial interests or personal relationships that could have appeared to influence the work reported in this paper.

Funding sources

This work was supported in part by grants from the Japanese Ministry of Education, Culture, Sports, Science, and Technology (Kakenhi Kiban C, 17K11802, to Shuhei Tsuchiya and Kakenhi Kiban B, 18H01732, to Kensuke Kuroda).

References

[1] A. Palmquist, O.M. Omar, M. Esposito, J. Lausmaa, P. Thomsen, Titanium oral implants: surface characteristics, interface biology and clinical outcome, J. R. Soc. Interface 7 Suppl 5 (2010) S515–S527.
[2] L. Linder, T. Albrektsson, P.I. Branemark, H.A. Hansson, B. Ivarsson, U. Jonsson, I. Lundstrom, Electron microscopic analysis of the bone-titanium interface, Acta Orthop. Scand. 54 (1) (1983) 45–52.
[3] C. Johansson, J. Lausmaa, M. Ask, H.A. Hansson, T. Albrektsson, Ultrastructural differences of the interface zone between bone and Ti 6Al 4V or commercially pure titanium, J. Biomed. Eng. 11 (1) (1989) 3–8.
[4] D.E. Steflik, G.R. Parr, A.L. Sisk, P.J. Hanes, F.T. Lake, Electron microscopy of bone response to titanium cylindrical screw-type endosseous dental implants, Int. J. Oral Maxillofac. Implant. 7 (4) (1992) 497–507.
[5] K. Murai, F. Takeshita, Y. Ayukawa, T. Kiyoshima, T. Suetsugu, T. Tanaka, Light and electron microscopic studies of bone-titanium interface in the tibiae of young and mature rats, J. Biomed. Mater. Res. 30 (4) (1996) 523–533.
[6] G. Sundell, C. Dahlin, M. Andersson, M. Thuvander, The bone-implant interface of dental implants in humans on the atomic scale, Acta Biomater. 48 (2017) 445–450.
[7] K. Sugimoto, S. Tsuchiya, M. Omori, R. Matsuda, M. Fujio, K. Kuroda, M. Okido, H. Hibi, Proteomic analysis of bone proteins adsorbed onto the surface of titanium dioxide, Biochem. Biophys. Rep. 7 (2016) 316–322.
[8] H.K. Nakamura, F. Butz, L. Saruwatari, T. Ogawa, A role for proteoglycans in mineralized tissue-titanium adhesion, J. Dent. Res. 86 (2) (2007) 147–152.
[9] J. Rnjak-Kovacina, F. Tang, J.M. Whitelock, M.S. Lord, Glycosaminoglycan and proteoglycan-based biomaterials: current trends and future perspectives, Adv. Healthc. Mater. 7 (6) (2018) e1701042.

[10] J.J. Collis, G. Embery, Adsorption of glycosaminoglycans to commercially pure titanium, Biomaterials 13 (8) (1992) 548–552.
[11] H. Nakamura, J. Shim, F. Butz, H. Aita, V. Gupta, T. Ogawa, Glycosaminoglycan degradation reduces mineralized tissue-titanium interfacial strength, J. Biomed. Mater. Res. A 77 (3) (2006) 478–486.
[12] M.M. Klinger, F. Rahemtulla, C.W. Prince, L.C. Lucas, J.E. Lemons, Proteoglycans at the bone-implant interface, Crit. Rev. Oral Biol. Med. 9 (4) (1998) 449–463.
[13] T. Albrektsson, Hard tissue implant interface, Aust. Dent. J. 53 Suppl 1 (2008) S34–S38.
[14] Y. Forster, C. Rentsch, W. Schneiders, R. Bernhardt, J.C. Simon, H. Worch, S. Rammelt, Surface modification of implants in long bone, Biomatter 2 (3) (2012) 149–157.
[15] T. Mikami, H. Kitagawa, Biosynthesis and function of chondroitin sulfate, Biochim. Biophys. Acta 1830 (10) (2013) 4719–4733.
[16] S. Yamauchi, S. Mita, T. Matsubara, M. Fukuta, H. Habuchi, K. Kimata, O. Habuchi, Molecular cloning and expression of chondroitin 4-sulfotransferase, J. Biol. Chem. 275 (12) (2000) 8975–8981.
[17] N. Hiraoka, H. Nakagawa, E. Ong, T.O. Akama, M.N. Fukuda, M. Fukuda, Molecular cloning and expression of two distinct human chondroitin 4-O-sulfotransferases that belong to the HNK-1 sulfotransferase gene family, J. Biol. Chem. 275 (26) (2000) 20188–20196.
[18] H.G. Kang, M.R. Evers, G. Xia, J.U. Baenziger, M. Schachner, Molecular cloning and characterization of chondroitin-4-O-sulfotransferase-3. A novel member of the HNK-1 family of sulfotransferases, J. Biol. Chem. 277 (38) (2002) 34766–34772.
[19] M.R. Evers, G. Xia, H.G. Kang, M. Schachner, J.U. Baenziger, Molecular cloning and characterization of a dermatan-specific N-acetylgalactosamine 4-O-sulfotransferase, J. Biol. Chem. 276 (39) (2001) 36344–36353.
[20] T. Mikami, S. Mizumoto, N. Kago, H. Kitagawa, K. Sugahara, Specificities of three distinct human chondroitin/dermatan N-acetylgalactosamine 4-O-sulfotransferases demonstrated using partially desulfated dermatan sulfate as an acceptor: implication of differential roles in dermatan sulfate biosynthesis, J. Biol. Chem. 278 (38) (2003) 36115–36127.
[21] M. Kluppel, The roles of chondroitin-4-sulfotransferase-1 in development and disease, Prog. Mol. Biol. Transl. Sci. 93 (2010) 113–132.
[22] A. Uccelli, L. Moretta, V. Pistoia, Mesenchymal stem cells in health and disease, Nat. Rev. Immunol. 8 (9) (2008) 726–736.
[23] M. Li, S. Ikehara, Bone-marrow-derived mesenchymal stem cells for organ repair, Stem Cells Int. 2013 (2013) 132642.
[24] D.M. Mosser, J.P. Edwards, Exploring the full spectrum of macrophage activation, Nat. Rev. Immunol. 8 (12) (2008) 958–969.
[25] S. Gordon, P.R. Taylor, Monocyte and macrophage heterogeneity, Nat. Rev. Immunol. 5 (12) (2005) 953–964.
[26] M. Genin, F. Clement, A. Fattaccioli, M. Raes, C. Michiels, M1 and M2 macrophages derived from THP-1 cells differentially modulate the response of cancer cells to etoposide, BMC Cancer 15 (2015) 577.
[27] A. Ruggeri, C. Dell'orbo, D. Quacci, Electron microscopic visualization of proteoglycans with Ruthenium Red, Histochem. J. 9 (2) (1977) 249–252.
[28] S. Bian, N. Akyuz, C. Bernreuther, G. Loers, E. Laczynska, I. Jakovcevski, M. Schachner, Dermatan sulfotransferase Chst14/D4st1, but not chondroitin sulfotransferase Chst11/C4st1, regulates proliferation and neurogenesis of neural progenitor cells, J. Cell Sci. 124 (Pt 23) (2011) 4051–4063.
[29] T. Albrektsson, P.I. Branemark, H.A. Hansson, J. Lindstrom, Osseointegrated titanium implants. Requirements for ensuring a long-lasting, direct bone-to-implant anchorage in man, Acta Orthop. Scand. 52 (2) (1981) 155–170.
[30] T. Albrektsson, M. Jacobsson, Bone-metal interface in osseointegration, J. Prosthet. Dent. 57 (5) (1987) 597–607.
[31] D.E. Steflik, A.L. Sisk, G.A. Parr, F.T. Lake, P.J. Hanes, Experimental studies of the implant-tissue interface, J. Oral Implantol. 19 (2) (1993) 90–94 discussion 136-7.
[32] K. Okamatsu, H. Kido, A. Sato, A. Watazu, M. Matsuura, Ultrastructure of the interface between titanium and surrounding tissue in rat tibiae–a comparison study on titanium-coated and -uncoated plastic implants, Clin. Implant Dent. Relat. Res. 9 (2) (2007) 100–111.
[33] T. Douglas, S. Heinemann, C. Mietrach, U. Hempel, S. Bierbaum, D. Scharnweber, H. Worch, Interactions of collagen types I and II with chondroitin sulfates A-C and their effect on osteoblast adhesion, Biomacromolecules 8 (4) (2007) 1085–1092.
[34] B. Stadlinger, V. Hintze, S. Bierbaum, S. Moller, M.C. Schulz, R. Mai, E. Kuhlisch, S. Heinemann, D. Scharnweber, M. Schnabelrauch, U. Eckelt, Biological functionalization of dental implants with collagen and glycosaminoglycans-A comparative study, J. Biomed. Mater. Res. B Appl. Biomater. 100 (2) (2012) 331–341.
[35] S. Rammelt, T. Illert, S. Bierbaum, D. Scharnweber, H. Zwipp, W. Schneiders, Coating of titanium implants with collagen, RGD peptide and chondroitin sulfate, Biomaterials 27 (32) (2006) 5561–5571.
[36] S. Bierbaum, T. Douglas, T. Hanke, D. Scharnweber, S. Tippelt, T.K. Monsees, R.H. Funk, H. Worch, Collageneous matrix coatings on titanium implants modified with decorin and chondroitin sulfate: characterization and influence on osteoblastic cells, J. Biomed. Mater. Res. A 77 (3) (2006) 551–562.
[37] P.J. Mroz, J.E. Silbert, Effects of [3H]glucosamine concentration on [3H]chondroitin sulphate formation by cultured chondrocytes, Biochem. J. 376 (Pt 2) (2003) 511–515.
[38] S. Shi, A.G. Chan, S. Mercer, G.J. Eckert, S.B. Trippel, Endogenous *versus* exogenous growth factor regulation of articular chondrocytes, J. Orthop. Res. 32 (1) (2014) 54–60.
[39] S. Mathews, S.A. Mathew, P.K. Gupta, R. Bhonde, S. Totey, Glycosaminoglycans enhance osteoblast differentiation of bone marrow derived human mesenchymal stem cells, J. Tissue Eng. Regen. Med. 8 (2) (2014) 143–152.
[40] B.L. Farrugia, M.S. Lord, J.M. Whitelock, J. Melrose, Harnessing chondroitin sulphate in composite scaffolds to direct progenitor and stem cell function for tissue repair, Biomater. Sci. 6 (5) (2018) 947–957.
[41] J.C.M. Souza, M.B. Sordi, M. Kanazawa, S. Ravindran, B. Henriques, F.S. Silva, C. Aparicio, L.F. Cooper, Nano-scale modification of titanium implant surfaces to enhance osseointegration, Acta Biomater. 94 (2019) 112–131.
[42] Q. Wang, Y. Huang, Z. Qian, Nanostructured surface modification to bone implants for bone regeneration, J. Biomed. Nanotechnol. 14 (4) (2018) 628–648.